PCCP

ROYAL SOCIETY OF CHEMISTRY

PAPER

View Article Online
View Journal

Cite this: DOI: 10.1039/d6cp00331a

Non-adiabatic origin of roaming OH dynamics in the formic acid dimer dication

Saroj Barik,†[a] Ester Livshits, †[ab] Roi Baer*[ab] and Daniel Strasser *[a]

Received 29th January 2026,
Accepted 27th April 2026

DOI: 10.1039/d6cp00331a

rsc.li/pccp

Ionization of molecular clusters can trigger chemical reactions and drive chemical evolution even at very low temperatures, influencing chemistry in interstellar, atmospheric, and planetary environments exposed to ionizing radiations. To investigate such processes involving the dissociation of both intramolecular and intermolecular bonds under controlled conditions, we examined the dynamics of the formic acid (FA) dimer dication in an ultrafast extreme-ultraviolet (EUV) pump and near-infrared (NIR) probe experiment, combined with *ab initio* molecular dynamics simulations. The dissociation of the intermolecular bond and the formation of the two-body $FA^+ + FA^+$ channel could be explained by ground-state dynamics, whereas the three-body breakup channels required a more detailed description. We developed a simplified dimer model for the breakup process that enabled non-adiabatic molecular dynamics simulations on excited-state CASPT2 potential energy surfaces, capturing both intermolecular and intramolecular dynamics. The simulations showed that immediately after the dimer dissociation and non-adiabatic decay to the ground electronic state, a roaming-OH mechanism develops, accounting for the observed kinetic-energy-release distributions and momentum correlations in the $FA^+ + CHO^+ + OH$ and $FA^+ + H_2O^+ + CO$ three-body breakup channels. The simplified modeling approach may serve as a practical framework for studying the excited-state dynamics in molecular dimer and cluster breakup processes.

Introduction

Ionization-induced molecular dynamics have profound implications on the chemical evolution of the interstellar medium and planetary atmosphere.[1–8] It can also initiate radiation damage processes in biological and materials systems.[9–12] Furthermore, the ionization of molecular clusters can be a powerful drive for the chemical evolution and formation of new bonds in dilute and cold environments, for example, the formation of aromatic bonds in the ionization of acetylene clusters[2] and peptide-bond formation on excited protonated serine dimer ions.[1] Ionization of symmetric dimer systems can result in symmetry-breaking dynamics due to asymmetric charge distributions in the ionized dimer.[3,13] The role of symmetry breaking underscores a long-debated question about the sequential *versus* concerted proton-transfer dynamics in dual hydrogen-bounded dimers, which are model systems for the studies of radiation damage to DNA base pairs.[14–26] One of the simplest examples of a dual hydrogen-bonded system is the formic acid (FA) dimer.[27] Our recent study[13] has combined *ab initio* molecular dynamics (AIMD) simulations with time-resolved ultrafast EUV pump–near-IR probe experiments to investigate its ionization-induced cation evolution, revealing proton transfer on both ultrafast and sub-picosecond time scales, as well as much slower dynamics, ultimately forming the protonated monomer FAH^+.

In planetary ionospheres and in the interstellar medium, abundant ionizing radiations can induce double ionization, triggering new reaction mechanisms in which Coulomb explosion (CE) often serves as the dominant pathway. However, in certain molecular systems, CE cannot occur directly and instead requires preceding structural rearrangements. For example, in the double ionization of some organic species leading to H_3^+ formation, CE is facilitated by the roaming of a neutral H_2 fragment that subsequently drives ultrafast ($\sim$100 fs) electron- or proton-transfer processes.[28–37] Moiety roaming, a widespread phenomenon following photoexcitation or photoionization, frequently gives rise to unexpected reaction products. In such cases, prolonged roaming of hydrogen atoms[38–43] or even heavier molecular fragments[44–56] can result in the formation of new bonds far from the initial location of the roaming moiety within the parent molecule.

The formic acid (FA) dimer has also served as a benchmark system for studying double ionization and Coulomb explosion in dual hydrogen-bonded complexes. These processes have been investigated using both intense laser fields and electron-impact ionization.[57–59] In particular, Zhou *et al.* reported ultrafast

[a] *Institute of Chemistry, The Hebrew University of Jerusalem, Jerusalem, 9190401, Israel. E-mail: strasser@huji.ac.il, roi.baer@mail.huji.ac.il*
[b] *Fritz Haber Research Center for Molecular Dynamics, The Hebrew University of Jerusalem, Jerusalem, 9190401, Israel*
† These authors contributed equally to this work.

intermolecular charge transfer induced sequential dissociation dynamics of the dimer, followed by the cleavage of C–H and C–O bonds, leading to complex fragmentation patterns of the FA_2^{2+} dimer dication formed upon electron-impact ionization.[57]

Here, we report on the dynamics of the formic acid dimer dication (FA_2^{2+}) produced by double-ionization with an ultrashort EUV pulse and probed by a time-delayed near-IR pulse. Coincidence 3D imaging measurements of the ionic products, combined with non-adiabatic *ab initio* molecular dynamics simulations on the ground and excited states of the dication revealed the non-adiabatic origin of OH-roaming dynamics that facilitates the measured $FA^+ + OH + CHO^+$ and $FA^+ + H_2O^+ + CO$ three-body product channels.

Results and discussion

The ionization of a molecular beam containing both FA monomers and dimers with broadband ultrashort EUV pulses produces multiple dissociative ionization and Coulomb explosion product channels.[13] Three-dimensional coincidence imaging enables the identification of ions originating from single-photon double-ionization of FA dimers.[29,30,60–63] The FA_2^{2+} dication KER spectra, measured for the only two-body fragmentation product channel, $FA^+ + FA^+$, and for three additional three-body channels, are shown as black lines in the four panels of Fig. 1. Panel (a) displays a narrow KER distribution peaking near 4 eV, with a total $FA^+ + FA^+$ coincidence yield of approximately 5% of all the measured FA_2^{2+} decays. The observed peak lies slightly higher than the ~3.6 eV reported for intense-laser ionization of the FA dimer.[59] This result is consistent with other studies showing that single-photon double ionization with EUV photons can produce higher KER values than sequential ionization in intense laser fields.[60,64–66]

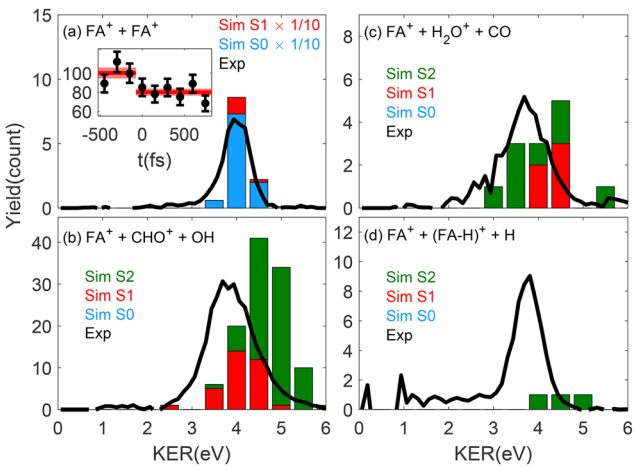

Fig. 1 Comparison of the measured (black lines) and simulated KER spectra of the two-body and three-body breakup channels of the FA dimer dication. (a) $FA^+ + FA^+$, inset showing the relative channel yield dependence on pump-probe delay, (b) $FA^+ + CHO^+ + OH$, (c) $FA^+ + H_2O^+ + CO$, and (d) $FA^+ + (FA–H)^+ + H$. Blue, red and green bars show simulated results from the S0, S1 and S2 states of FA_2^{2+} immediately after ionization. Experimental yields are in counts per 24 h acquisition time; simulated yields indicate the number of breakup trajectories (out of 100 per initial state) falling into each KER bin. The simulated yields in panel (a) are multiplied by factor 1/10 to match with experimental yield scale.

Our experimental measurements can be directly compared with simulated dynamics initiated on the low-lying excited states of the dication, produced by single-photon double ionization with a broadband ultrashort EUV pulse.[60] Accurate modeling of the FA_2^{2+} excited-state dynamics requires high-level quantum-chemical methods such as CASPT2, but for molecular clusters, this approach is typically far too costly for generating a representative ensemble of molecular-dynamics trajectories. It can, however, be applied to single-point FA_2^{2+} calculations at a limited set of initial geometries near the Franck–Condon region. These calculations showed that immediately after double ionization, the system exhibits an initially symmetric charge separation. One hole is localized on the carbon atom of each monomer both for the dication ground state and for the low-lying excited electronic states. The two holes do not overlap spatially, and the energy splittings between the corresponding singlet and triplet eigenstates are very small (0.01–0.05 eV; for details, see the SI). Together, these observations indicate that the intermonomer coupling is predominantly electrostatic and motivate an approximate modelling strategy in which one FA^+ monomer is treated quantum-mechanically, whereas the second monomer is represented as a movable point mass and charge. This approach made it possible to simulate high-level non-adiabatic dynamics on the three lowest electronic states: the ground state S0 and the two lowest excited states S1 and S2. In all three states, the explicit monomers are in a doublet spin state. Fig. 2 shows the snapshots of simulated FA dimer geometries, indicating the position of the 46 amu ion that is placed at the position of the central carbon atom of one of the FA monomers. The principal approximation in this model is the neglect of hydrogen bonding between the monomers, which can lead to differences in the energetics of the ground state and the two excited states. Using this quantum-chemical model, we performed non-adiabatic *ab initio* molecular-dynamics (NA-AIMD) simulations in which both the explicit monomer cation and the movable charge representing the partner monomer were included. Further computational details and checks of the model validity, including simulations of FA^+ monomers without a point charge, are provided in the SI and Methods section.

The simulated KER spectrum of the two-body breakup channel is shown in Fig. 1a. It exhibits a narrow distribution peaking at 4 eV, in good agreement with the experimental data. The blue bars represent contributions from simulated trajectories on the S0 potential surface of the explicit monomer cation. All 100 S0 trajectories led to the two-body $FA^+ + FA^+$ dissociation channel. This was seen for the CASPT2 trajectories in the simple monomer model and also for DFT simulations of the triplet FA_2^{2+} ground-state dynamics, where both monomers were fully represented. The DFT calculations of the singlet ground-state dynamics were discarded because of their non-single-determinant nature. Using NA-AIMD, we found that the dynamics on the first excited state (S1) contribute only weakly to this two-body $FA^+ + FA^+$ channel, as indicated by the red bars in Fig. 1a.

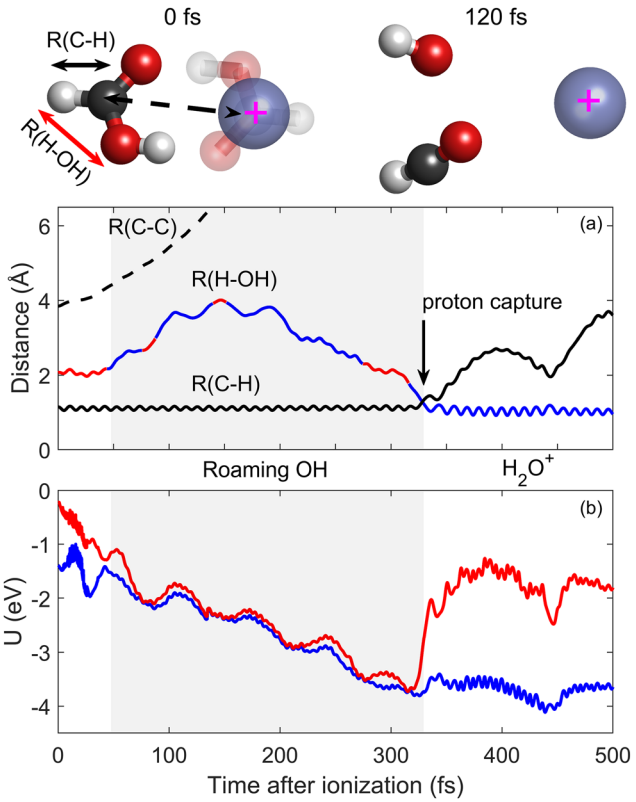

Fig. 2 Typical H_2O-forming NA-AIMD trajectory that is initiated on the S_1 state of the dimer dication. The initial FA_2^{2+} geometry at 0 fs and 120 fs after ionisation is shown, where one of the FA^+ molecules is modelled with an equivalent 46 amu cation. (a) Selected atomic distances as a function of time after ionization: solid and dashed black curves show the C–H and C–C distances, respectively. Color-coded curve shows the H–OH distance, and its colour indicates the instantaneous electronic adiabatic state, with S1 represented by red and S0 by blue. (b) S1 (in red) and S0 (in blue) potential energies along the same trajectory. Shaded region indicates the OH-roaming time until the formation of the H_2O^+ product by proton capture and its dissociation from the CO moiety.

The inset in Fig. 1a shows the measured effect of introducing a time-resolved near-IR probe on the ionization-induced dynamics. For the two-body $FA^+ + FA^+$ product channel, the time-delayed probe reduced the channel yield by about 20%. We attributed the reduced yield to enhanced electronic excitation of the dication by the near-IR pulse, thus supporting the theoretical prediction that the two-body channel originates primarily from the ground-state dynamics.

The dominant three-body breakup channel (33% of all dication fragmentation events) is $FA^+ + CHO^+ + OH$, exhibiting the breakup of the intramolecular C–O bond in addition to the dimer dissociation. Its experimental KER distribution, shown in Fig. 1b, peaks at 3.9 eV and is markedly broader than that of the two-body channel. The simulations showed that this channel is obtained only for dynamics initiated on excited electronic states (S1 and S2) with a broad distribution similar to that of the experiment. Trajectories initiated on S1 reproduce the experimental KER distribution well, whereas those from the S2 peak ~0.9 eV higher. Consequently, the total simulated distribution (S1 + S2) is pulled toward higher KER. This discrepancy likely arises from our assumption of equal initial populations for S1 and S2 (whereas double-ionization by the EUV pulse may favour S1) and/or from the reduced-dimensionality model, in which one FA monomer is treated as a movable point charge, and thus may underestimate the dissipation of excess energy into its internal vibrational modes.

The dissociation of the C–O bond can also be accompanied by additional structural rearrangement and the formation of the H_2O^+ product. The KER distribution of the $FA^+ + H_2O^+ + CO$ channel peaks at 3.8 eV and is similarly broad, though ~10 times weaker in yield than the $FA^+ + CHO^+ + OH$ channel, as shown in Fig. 1b. Simulations indicate that this pathway likewise requires the population of the excited states. The relative calculated yields of these three-body channels closely follow the experimental ones. This stands in contrast to the overestimated two-body breakup simulated in Fig. 1a, which must be scaled by 1/10 to match the average number of $FA^+ + FA^+$ events per 24 h measurement time.

In our earlier single-photon double ionization studies in methanol, we found uniform population of the low-lying singlet dication states.[60] However, the strong dominance of the three-body breakup channels indicates that double ionization of the formic acid dimer by the EUV pulse preferentially populates excited dication states rather than the ground state. This can be explained by a mechanism in which one monomer is initially doubly ionized, followed by ultrafast intermolecular charge transfer,[57] or by intermolecular coulombic decay (ICD)[58,67] following an initial single-ionization of an inner level by the EUV pulse. These electronic decay processes typically occur on a fs or sub-fs timescale, effectively setting the "time zero" for subsequent nuclear dynamics before any significant structural rearrangement can occur. The rapid transition to excited states accounts for the relatively low yield of the two-body breakup channel, which the current model attributes mainly to ground-state dynamics.

The last three-body breakup channel exhibits H atom ejection from one of the dissociating monomers. Fig. 1d shows the measured KER spectrum of the $FA^+ + (FA–H)^+ + H$ channel, exhibiting a narrow distribution peaking at ~3.8 eV, similar to the two-body channel. This channel was measured with similar yields as the two-body channel; nevertheless, it occurred in only 3 simulated trajectories on the S2 excited state. Zhou *et al.* reported the same channel in electron-impact double ionization experiments and attributed it to sequential dissociation of the C–H bond on one of the FA^+ monomers following the dimer breakup.[57] To account for the excess excitation of electronic degrees of freedom and reproduce the C–H dissociation, Zhou *et al.* performed theoretical ground-state simulations, including the addition of 5.44 eV vibrational energy to FA_2^{2+}.[57] The S2 state lies only ~3.2 eV above the dication ground state, and it is therefore possible that the main contribution to H dissociation is associated with higher lying potentials that were not considered here. Higher lying potentials are also likely to be involved in the observed four-body breakup channels. For example, the prominent $(FA–H)^+ + H + CHO^+ + OH$ channel involves the dissociation of both FA monomers. See the SI for the complete branching ratios of all the measured CE channels.

The observed H_2O^+ products indicate a particularly non-trivial dissociation mechanism. Earlier studies of intense laser ionization of the FA monomer reported H_2O^+ formation and attributed it to the migration of the H atom from the C atom to the OH.[68] Nevertheless, its production in FA dimer ionization was not considered in the earlier experimental and theoretical studies.[57–59] One can tentatively consider several mechanisms that could form H_2O^+, starting from the initial geometry in which the two H atoms are separately situated in the CH and the OH moieties. An H-migration mechanism can be proposed, conversely, the heavier OH moiety can migrate towards the H atom on the other side of the FA monomer.[45–48,68] Fig. 2 shows a typical H_2O^+ forming trajectory that was initiated on the S1 state. The dashed line in Fig. 2a shows the simulated C–C distance (represented by the distance between the carbon atom of the explicit monomer and the position of the movable charge) that exhibits a direct ultrafast dissociation of the FA_2^{2+} dimer. In contrast, the C–H bond, indicated by the full black line, remains stable at ~1 Å, until a secondary dissociation occurs at ~330 fs after ionization. The mechanism becomes clear when we consider the H–OH distance as a function of time after ionization, indicated by the color-coded curve. Initially on the S1 state, the H–OH distance remains stable at ~2 Å, reflecting the distance between the OH moiety and the second H that is bound to the carbon in the neutral FA monomer. After the dimer dissociation is well on its way, at ~44 fs, we observe a non-adiabatic transition from the S1 state to the S0 ground state, labelled, respectively, with red- and blue-coloured lines. As seen in Fig. 2b, at that time, the S1 and S0 potentials pass very close to a conical intersection that facilitates the non-adiabatic transition. On S0, the H–OH distance grows, as can be seen in Fig. 2 showing the FA_2^+ geometry snapshot taken 120 fs after ionization. The H–OH distance exhibits oscillations on a ~40 fs time scale as the OH moiety roams around the monomer until it reaches the H atom on the other side. During the OH roaming, S1 and S0 become nearly degenerate, as the spin direction of the OH radical does not affect the potential of the distant CHO^+. However, as OH captures a proton and dissociates, the degeneracy is lifted and the H–OH distance exhibits vibrational oscillations around the characteristic length of ~1 Å of the OH bond of H_2O^+.[69] The supplementary video file shows a molecular dynamics movie of this typical trajectory, clearly exhibiting roaming OH dynamics. This scenario concerning the onset of roaming is also typical for the dynamics initiated on the S2 state. In both initially excited states, the secondary dissociation of the H_2O^+ product occurred after a long time, up to 1 ps after ionization. More details about the simulated ensemble are provided in the SI.

When considering the combined yield of all three-body and four-body C–O bond breaking channels, we observed (as shown in the SI) few percent enhancement for positive probe delays, further supporting the theoretical prediction that the intermolecular fragmentation originates from excited-state dynamics. Additional time-resolved insights can be obtained by comparing the measured and simulated momentum correlations of the three-body breakup events[70] shown in Fig. 3, where three-body momentum correlations are shown using the mass-scaled Dalitz plot representation. Fig. 3a shows the mapping of momentum

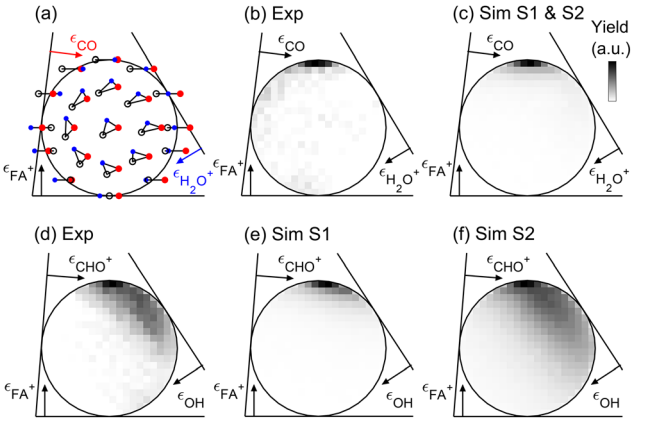

Fig. 3 Three-body momentum correlations for the FA^+ + CHO^+ + OH and FA^+ + H_2O^+ + CO channels. (a) Mapping of FA^+ + H_2O^+ + CO momentum correlations onto the mass-scaled Dalitz plot representation. (b) and (c) Measured and simulated correlations of the FA^+ + H_2O^+ + CO channel. (d) Measured correlations of the FA^+ + CHO^+ + OH channel. (e) and (f) Simulated correlations for the trajectories of the same channel initiated on the S1 and S2 states, respectively.

correlations for FA^+ + H_2O^+ + CO dissociation events. Three correlated kinetic energy fraction axes ε_{FA^+}, $\varepsilon_{H_2O^+}$ and ε_{CO} are indicated, corresponding to the kinetic energy fraction of each fragment, scaled by the maximal possible fraction of each mass while conserving the total momentum in the center of mass frame. An uncorrelated three-body breakup would appear as a uniform distribution inside the unit circle. In contrast, the measured FA^+ + H_2O^+ + CO events exhibit a highly correlated distribution that is shown in Fig. 3b. In this channel, the FA^+ ions carry nearly the maximum possible kinetic energy while the remaining energy is randomly distributed between the H_2O^+ and CO products. This momentum correlation is typical for sequential dissociation,[30,62,71] in which an initial dissociation releases most of the available energy in a FA^+–FA^+ Coulomb explosion. The secondary dissociation occurs after a sufficiently long time-delay, allowing for the loss of correlation between the angle of the H_2O^+ + CO dissociation vector and the direction of the intact FA^+ fragment. The same correlations can be seen in the simulated momentum correlations of the roaming OH dynamics, resulting in the FA^+ + H_2O^+ + CO channel shown in Fig. 3c.

It is also interesting to consider the measured 3-body momentum correlations of the FA^+ + CHO^+ + OH channel, as shown in Fig. 3d. Similar to the H_2O^+ formation channel, the distribution peaks at the maximal possible FA^+ energy fraction. However, for events with lower ε_{FA^+}, the remaining energy is not randomly shared between CHO^+ and OH and is preferentially carried by the ε_{CHO^+} product. This suggests a different scenario, in which the second dissociation step can occur on a faster time scale that does not allow the loss of correlation due to the rotation of the C–O bond direction with respect to the direction of the dissociating FA^+ monomer. Furthermore, in such an early dissociation scenario, the ionic CHO^+ product can still gain additional kinetic energy due to the long-range repulsion from the FA^+ fragment. Fig. 3e and f show the simulated momentum correlations for the FA^+ + CHO^+ + OH channel, initiated, respectively,

on the S1 and S2 states. Trajectories starting on the S1 state reproduce the peak of the measured distribution attributed to long-time delay between the intermolecular dissociation and the intramolecular dissociation, while the S2 trajectories reproduce the correlated intermolecular and intramolecular bonds. Indeed, the analysis of the simulated trajectory ensemble shown in the SI demonstrates that roaming OH events initiated on S1 can culminate, up to 1 ps after ionization, upon release of the roaming neutral OH moiety rather than proton transfer and H_2O^+ formation. Most trajectories initiated on the S2 state exhibit a faster OH release within the first 100 fs, making it difficult to clearly assign the characteristic roaming OH motion.

Conclusions

In summary, the ultrafast intermolecular and intramolecular fragmentation dynamics of FA_2^{2+} dimers were studied by double-ionization in ultrafast EUV pump – near-IR probe experiments. Then, 3D coincidence imaging measurements of the two-body and three-body breakup channels were directly compared with the NA-AIMD simulations of excited-state dynamics. The three-body momentum correlations reveal a rich roaming OH dynamics that are initiated after the dissociation of the dimer and the non-adiabatic transition of initially electronically excited dication to the ground-electronic state on which the roaming occurs. The success of the simulations to predict channel-resolved kinetic energy release, H_2O^+ *vs.* OH relative yields and momentum correlations in three-body breakup channels validates the chosen theoretical model that simplifies the cluster dynamics by considering one of the monomers as a point charge, while conserving the high-level electronic-structure calculation and non-adiabatic dynamics. We found not only that the H_2O^+ formation is facilitated by the roaming of the heavier OH moiety, rather than the migration of a lighter H atom, but also that the ejection of neutral OH proceeds similarly *via* the roaming OH mechanism. Further studies are required to explore and validate the approach for the simplified simulation of excited-state dynamics in other molecular cluster systems, as well as to elucidate the role of roaming OH dynamics in other systems that exhibit competing H_2O^+ and OH production.

Methods

Experimental methods

The experimental setup and methodology have been described in the earlier work.[13,60–63] The molecular beam of formic acid dimers was produced in an effusive beam, formed by room-temperature vapor pressure of FA passed through a 200 micron aperture.[13] Ultrashort EUV pulses were produced by HHG in a semi-infinite Argon gas cell,[72,73] and were spatially filtered from the fundamental 800 nm laser of 35 fs pulse. The broad-bandwidth EUV pulses, extending up to ~40 eV,[73] initiated dynamics on the ground and excited states of the FA_2^{2+} dication by single-photon double-ionization, or by single ionization of an inner electron followed by a nearly instantaneous ICD. The dynamics were probed by a time-delayed near-IR pulse, mildly focused to ~0.5 mm diameter and merged with the EUV pulse in the interaction region. The ionic products were accelerated to a time- and position-sensitive MCP detector, equipped with a phosphor anode. The timing information was read out by a fast scope, and position information was acquired optically. Gain amplitude fluctuations were used to correlate time and position information.[74–77] Then, 3D ion momenta were extracted from the ion recoil position in the detector plane and ion recoil in the time-of-flight direction. In the three-body breakup channels, the neutral fragment momentum was calculated from the ion center of mass recoil in the lab frame,[60] thus making it possible to measure the channel-resolved KER distributions and three-body momentum correlations.[30,60,62] The reported data were acquired at a 1 kHZ repetition rate over a period of 56 days, while scanning the near-IR delay in 50 fs steps.

Computational methods

NA-AIMD. The calculations were performed in three stages:

(1) Thermalized initial conditions. The long-duration *ab initio* molecular dynamics (AIMD) simulation of the neutral FA dimer was performed at 300 K using the DFT/BNL* functional (with range-separation parameter γ = 0.417 a_0^{-1}, determined by tuning[78–80]) and the aug-cc-pVDZ basis set, as implemented in Q-Chem 5.4.[81] From this trajectory, 100 well-separated snapshots—chosen after the decay of temporal correlations—were extracted to represent a thermalized ensemble of initial geometries.

(2) Replacement of one formic acid monomer by a dummy atom. For each initial condition, one formic acid molecule was replaced by a movable charge carrying the same net positive charge and mass as the monomer. The movable charge was positioned at the location of the carbon atom of the original acid molecule.

(3) Nonadiabatic *ab initio* molecular dynamics (NA-AIMD). Each of the 100 configurations generated in Stage 2 was used to initiate nonadiabatic molecular dynamics (MD) calculations on each of the three lowest-lying dicationic electronic states, yielding a total of 300 trajectories. The nonadiabatic dynamics were treated using surface-hopping molecular dynamics trajectories[82] generated at the XMS-CASPT2/(13e,9o)/aug-cc-pVDZ/density-fitting level using the BAGEL electronic structure package.[83] The single-state single-reference (SS-SR) contraction scheme[84,85] was employed, with a vertical shift set to 0.2 E_h. BAGEL was interfaced with Newton-X (v2.2)[86] to perform the surface-hopping NA-AIMD,[87] using a time step of 0.3 fs. Transitions were restricted to hops between the adjacent electronic states due to computational constraints. The *ab initio* dynamics were propagated for up to 1 ps or until the interfragment velocities reached an asymptotic, monotonic regime. At this point, the residual long-range Coulomb repulsion was accounted for by propagating the centers of mass of the resulting cationic fragments using classical equations of motion.

Fully atomistic DFT AIMD reference simulations

In addition to the NA-AIMD calculations, fully atomistic DFT AIMD simulations were carried out assuming a triplet ground electronic state, with both FA monomers explicitly represented.

The same electronic structure package and DFT methodology described in stage 1 were employed. The simulations were initiated from the same 100 well-separated snapshots described in stage 1, and all trajectories were propagated for 1 ps.

Author contributions

Saroj Barik: conceptualization, data curation, formal analysis, investigation, methodology, software, validation, visualization, writing – original draft, writing – review & editing. Ester Livshits: conceptualization, data curation, formal analysis, investigation, methodology, software, validation, visualization, writing – review & editing. Roi Baer: conceptualization, formal analysis, funding acquisition, investigation, methodology, project administration, resources, software, supervision, validation, visualization, writing – review & editing. Daniel Strasser: conceptualization, data curation, formal analysis, funding acquisition, investigation, methodology, project administration, resources, software, supervision, validation, visualization, writing – original draft, writing – review & editing.

Conflicts of interest

There are no conflicts to declare.

Data availability

The data supporting this study are available within the main text and the supplementary information (SI). Supporting information includes the following chapters: measured product branching ratios in the formic acid dimer dication breakup; measured yields as a function of EUV pump – near-IR probe delay; typical roaming OH trajectory simulation, forming a neutral OH product; typical H_2O^+ forming trajectory, initiated on the S2 state; simulated trajectory ensemble; Mulliken Charge and Excited-State Energetics Analyses of states FA_2^{+2}; the effect of one FA^+ monomer on the dissociation of the second FA^+. See DOI: https://doi.org/10.1039/d6cp00331a.

Acknowledgements

The authors acknowledge the support from ISF grants 1153/23 and 2539/25 as well as support from the Minerva Center for Making Bonds by Fragmentation. S.B. acknowledges the support provided by the Lady Davis Fellowship.

References

1 O. Licht, D. Barreiro-Lage, P. Rousseau, A. Giuliani, A. R. Milosavljević, A. Isaak, Y. Mastai, A. Albeck, R. Singh, V. T. T. Nguyen, L. Nahon, L. Martínez-Fernández, S. Díaz-Tendero and Y. Toker, Peptide Bond Formation in the Protonated Serine Dimer Following Vacuum UV Photon-Induced Excitation, *Angew. Chem. Int. Ed.*, 2023, **62**(15), e202218770, DOI: 10.1002/anie.202218770.

2 T. Stein, B. Bandyopadhyay, T. P. Troy, Y. Fang, O. Kostko, M. Ahmed and M. Head-Gordon, Ab Initio Dynamics and Photoionization Mass Spectrometry Reveal Ion-Molecule Pathways from Ionized Acetylene Clusters to Benzene Cation, *Proc. Natl. Acad. Sci. U. S. A.*, 2017, **114**(21), E4125–E4133, DOI: 10.1073/pnas.1616464114.

3 E. Livshits, D. M. Bittner, F. Trost, S. Meister, H. Lindenblatt, R. Treusch, K. Gope, T. Pfeifer, R. Baer, R. Moshammer and D. Strasser, Symmetry-Breaking Dynamics of a Photoionized Carbon Dioxide Dimer, *Nat. Commun.*, 2024, **15**(1), 6322, DOI: 10.1038/s41467-024-50759-2.

4 J. Londoño-Restrepo, S. Gómez, H. M. Quitián-Lara, F. Fantuzzi and A. Restrepo, More π, Please: What Drives the Formation of Unsaturated Molecules in the Interstellar Medium?, *Chem. Sci.*, 2025, **16**(7), 3051–3065, DOI: 10.1039/d4sc07986h.

5 M. Gatchell, R. Delaunay, G. D'Angelo, A. Mika, K. Kulyk, A. Domaracka, P. Rousseau, H. Zettergren, B. A. Huber and H. Cederquist, Ion-Induced Molecular Growth in Clusters of Small Hydrocarbon Chains, *Phys. Chem. Chem. Phys.*, 2017, **19**(30), 19665–19672, DOI: 10.1039/c7cp02090b.

6 S. Ganguly, D. Barreiro-Lage, N. Walsh, B. Oostenrijk, S. L. Sorensen, S. Díaz-Tendero and M. Gisselbrecht, The Origin of Enhanced O2+ Production from Photoionized CO2 Clusters, *Commun. Chem.*, 2022, **5**, 16, DOI: 10.1038/s42004-022-00629-z.

7 T. Matsubara, Theoretical Insights into a Novel Ion-Ion Reaction of Methane in the Initial Stages of Hydrocarbon Growth in Space, *ACS Earth Space Chem.*, 2024, **8**(12), 2557–2573, DOI: 10.1021/acsearthspacechem.4c00242.

8 A. Daniely, A. Wannenmacher, N. Levy, O. Sheffer, E. Joseph, O. Kostko, M. Ahmed and T. Stein, A Vacuum Ultraviolet Photoionization Mass Spectrometry and Density Functional Calculation Study of Formic Acid-Water Clusters, *J. Phys. Chem. A*, 2024, **128**(31), 6392–6401, DOI: 10.1021/acs.jpca.4c02875.

9 E. Alizadeh, T. M. Orlando and L. Sanche, Biomolecular Damage Induced by Ionizing Radiation: The Direct and Indirect Effects of Low-Energy Electrons on DNA, *Annu. Rev. Phys. Chem.*, 2015, **66**, 379–398, DOI: 10.1146/annurev-physchem-040513-103605.

10 U. Hergenhahn, Production of Low Kinetic Energy Electrons and Energetic Ion Pairs by Intermolecular Coulombic Decay, *Int. J. Radiat. Biol.*, 2012, **88**, 871–883, DOI: 10.3109/09553002.2012.698031.

11 A. Yokoya and T. Ito, Photon-Induced Auger Effect in Biological Systems: A Review, *Int. J. Radiat. Biol.*, 2017, 743–756, DOI: 10.1080/09553002.2017.1312670.

12 J. D. Asmussen, A. R. Abid, A. Sundaralingam, B. Bastian, K. Sishodia, S. De, L. Ben Ltaief, S. Krishnan, H. B. Pedersen and M. Mudrich, Secondary Ionization of Pyrimidine Nucleobases and Their Microhydrated Derivatives in Helium Nanodroplets, *Phys. Chem. Chem. Phys.*, 2023, **25**(36), 24819–24828, DOI: 10.1039/d3cp02879h.

13 S. Barik, E. Livshits, R. Baer and D. Strasser, Ultrafast and Ultraslow Proton-Transfer Dynamics Induced by Formic Acid Dimer Ionization, *J. Phys. Chem. A*, 2025, **16**, 37, DOI: 10.1021/acs.jpca.5c02619.

14 W. J. Schreier, P. Gilch and W. Zinth, Early Events of DNA Photodamage, *Annu. Rev. Phys. Chem.*, 2015, **66**, 497–519, DOI: 10.1146/annurev-physchem-040214-121821.
15 P.-O. Löwdin, Proton Tunneling in DNA and Its Biological Implications, *Rev. Mod. Phys.*, 1963, **35**(3), 724–732, DOI: 10.1103/RevModPhys.35.724.
16 J. D. Watson and F. H. C. Crick, Molecular Structure of Nucleic Acids: A Structure for Deoxyribose Nucleic Acid, *Nature*, 1953, **171**(4356), 737–738, DOI: 10.1038/171737a0.
17 Y. Kim, Direct Dynamics Calculation for the Double Proton Transfer in Formic Acid Dimer, *J. Am. Chem. Soc.*, 1996, **118**(6), 1522–1528, DOI: 10.1021/ja953175v.
18 S. D. Ivanov, I. M. Grant and D. Marx, Quantum Free Energy Landscapes from Ab Initio Path Integral Metadynamics: Double Proton Transfer in the Formic Acid Dimer Is Concerted but Not Correlated, *J. Chem. Phys.*, 2015, **143**(12), 124304, DOI: 10.1063/1.4931052.
19 H. Ushiyama and K. Takatsuka, Successive Mechanism of Double-Proton Transfer in Formic Acid Dimer: A Classical Study, *J. Chem. Phys.*, 2001, **115**(13), 5903–5912, DOI: 10.1063/1.1398090.
20 J. Kohanoff, S. Koval, D. A. Estrin, D. Laria and Y. Abashkin, Concertedness and Solvent Effects in Multiple Proton Transfer Reactions: The Formic Acid Dimer in Solution, *J. Chem. Phys.*, 2000, **112**(21), 9498–9508, DOI: 10.1063/1.481585.
21 H. Tachikawa, Proton Transfer vs Complex Formation Channels in Ionized Formic Acid Dimer: A Direct Ab Initio Molecular Dynamics Study, *J. Phys. Chem. A*, 2020, **124**(16), 3048–3054, DOI: 10.1021/acs.jpca.0c01729.
22 W. Li, L. Evangelisti, Q. Gou, W. Caminati and R. Meyer, The Barrier to Proton Transfer in the Dimer of Formic Acid: A Pure Rotational Study, *Angew. Chem.*, 2019, **131**(3), 869–875, DOI: 10.1002/ange.201812754.
23 S. F. Sutton, C. H. Rotteger, C. K. Jarman, P. Tarakeshwar and S. G. Sayres, Ultrafast Proton Transfer and Contact Ion-Pair Formation in Formic Acid Clusters, *J. Phys. Chem. Lett.*, 2023, **14**(37), 8306–8311, DOI: 10.1021/acs.jpclett.3c01654.
24 K. Mackeprang, Z. H. Xu, Z. Maroun, M. Meuwly and H. G. Kjaergaard, Spectroscopy and Dynamics of Double Proton Transfer in Formic Acid Dimer, *Phys. Chem. Chem. Phys.*, 2016, **18**(35), 24654–24662, DOI: 10.1039/c6cp03462d.
25 H. Sekiya and K. Sakota, Excited-State Double-Proton Transfer in a Model DNA Base Pair: Resolution for Stepwise and Concerted Mechanism Controversy in the 7-Azaindole Dimer Revealed by Frequency- and Time-Resolved Spectroscopy, *J. Photochem. Photobiol., C*, 2008, 81–91, DOI: 10.1016/j.jphotochemrev.2008.04.001.
26 R. Crespo-Otero, N. Kungwan and M. Barbatti, Stepwise Double Excited-State Proton Transfer Is Not Possible in 7-Azaindole Dimer, *Chem. Sci.*, 2015, **6**(10), 5762–5767, DOI: 10.1039/c5sc01902h.
27 P. Farfán, A. Echeverri, E. Diaz, J. D. Tapia, S. Gómez and A. Restrepo, Dimers of Formic Acid: Structures, Stability, and Double Proton Transfer, *J. Chem. Phys.*, 2017, **147**(4), 044312, DOI: 10.1063/1.4985880.
28 E. Livshits, I. Luzon, K. Gope, R. Baer and D. Strasser, Time-Resolving the Ultrafast H2 Roaming Chemistry and H3+ Formation Using Extreme-Ultraviolet Pulses, *Commun. Chem.*, 2020, **3**(1), 49, DOI: 10.1038/s42004-020-0294-1.
29 D. Strasser, E. Livshits and R. Baer, Single-Photon Double-Ionisation Coulomb Explosion in Organic Molecules, *Int. Rev. Phys. Chem.*, 2023, **42**(1–4), 29–51, DOI: 10.1080/0144235X.2023.2450916.
30 K. Gope, D. M. Bittner and D. Strasser, Sequential Mechanism in H 3 + Formation Dynamics on the Ethanol Dication, *Phys. Chem. Chem. Phys.*, 2023, **25**(9), 6979–6986, DOI: 10.1039/d2cp03632k.
31 K. Gope, E. Livshits, D. M. Bittner, R. Baer and D. Strasser, Two Pathways and an Isotope Effect in H3+ Formation Following Double Ionization of Methanol, *Nat. Sci.*, 2021, **1**(2), e10022, DOI: 10.1002/ntls.10022.
32 K. Gope, E. Livshits, D. M. Bittner, R. Baer and D. Strasser, An "Inverse" Harpoon Mechanism, *Sci. Adv.*, 2022, **8**(39), 8084, DOI: 10.1126/sciadv.abq8084.
33 D. Mishra, A. C. LaForge, L. M. Gorman, S. Díaz-Tendero, F. Martín and N. Berrah, Direct Tracking of H2 Roaming Reaction in Real Time, *Nat. Commun.*, 2024, **15**(1), 6656, DOI: 10.1038/s41467-024-49671-6.
34 A. Ngai, S. Hartweg, J. D. Asmussen, B. Bastian, M. Bonanomi, C. Callegari, M. Danailov, M. di Fraia, R. Feifel, S. D. Ganeshamandiram, S. Krishnan, A. LaForge, F. Landmesser, L. B. Ltaief, M. Michelbach, N. Pal, O. Plekan, N. Rendler, L. Raimondi, F. Richter, A. Scognamiglio, T. Sixt, R. J. Squibb, K. Dulitz, F. Stienkemeier and M. Mudrich, Roaming Dynamics in the Formation of Following Two-Photon Double Ionization of Ethanol and Aminoethanol, *Sci. Rep.*, 2025, **15**(1), 3201, DOI: 10.1038/s41598-024-84531-9.
35 N. Ekanayake, T. Severt, M. Nairat, N. P. Weingartz, B. M. Farris, B. Kaderiya, P. Feizollah, B. Jochim, F. Ziaee, K. Borne, P. K. Raju, K. D. Carnes, D. Rolles, A. Rudenko, B. G. Levine, J. E. Jackson, I. Ben-Itzhak and M. Dantus, H2 Roaming Chemistry and the Formation of H3+ from Organic Molecules in Strong Laser Fields, *Nat. Commun.*, 2018, **9**(1), 5186, DOI: 10.1038/s41467-018-07577-0.
36 K. Yoshikawa, M. Kanno, H. Xue, N. Kishimoto, S. Goto, F. Ota, Y. Tamura, F. Trinter, K. Fehre, L. Kaiser, J. Stindl, D. Tsitsonis, M. Schöffler, R. Dörner, R. Boll, B. Erk, T. Mazza, T. Mullins, D. E. Rivas, P. Schmidt, S. Usenko, M. Meyer, E. Wang, D. Rolles, A. Rudenko, E. Kukk, T. Jahnke, S. Díaz-Tendero, F. Martín, K. Hatada and K. Ueda, Time-Resolved Photoelectron Diffraction Imaging of Methanol Photodissociation Involving Molecular Hydrogen Ejection, *Phys. Chem. Chem. Phys.*, 2024, **26**(38), 25118–25130, DOI: 10.1039/d4cp01015a.
37 E. Wang, N. G. Kling, A. C. LaForge, R. Obaid, S. Pathak, S. Bhattacharyya, S. Meister, F. Trost, H. Lindenblatt, P. Schoch, M. Kübel, T. Pfeifer, A. Rudenko, S. Díaz-Tendero, F. Martín, R. Moshammer, D. Rolles and N. Berrah, Ultrafast Roaming Mechanisms in Ethanol Probed by Intense Extreme Ultraviolet Free-Electron Laser Radiation: Electron Transfer *versus* Proton Transfer, *J. Phys. Chem. Lett.*, 2023, **14**(18), 4372–4380, DOI: 10.1021/acs.jpclett.2c03764.
38 D. Townsend, S. A. Lahankar, S. K. Lee, S. D. Chambreau, A. G. Suits, X. Zhang, J. Rheinecker, L. B. Harding and

J. M. Bowman, The Roaming Atom: Straying from the Reaction Path in Formaldehyde Decomposition, *Science*, 2004, **306**(5699), 1158–1161, DOI: 10.1126/science.1104386.

39 A. G. Suits, Roaming Atoms and Radicals: A New Mechanism in Molecular Dissociation, *Acc. Chem. Res.*, 2008, **41**(7), 873–881, DOI: 10.1021/ar8000734.

40 S. A. Lahankar, S. D. Chambreau, D. Townsend, F. Suits, J. Farnum, X. Zhang, J. M. Bowman and A. G. Suits, The Roaming Atom Pathway in Formaldehyde Decomposition, *J. Chem. Phys.*, 2006, **125**(4), 044303, DOI: 10.1063/1.2202241.

41 Y. L. Fu, Y. Bai, Y. C. Han, B. Fu and D. H. Zhang, Double-Roaming Dynamics in the H + C2H2→ H2+ C2H Reaction: Acetylene-Facilitated Roaming and Vinylidene-Facilitated Roaming, *J. Phys. Chem. Lett.*, 2021, **12**(17), 4211–4217, DOI: 10.1021/acs.jpclett.1c01045.

42 Á. Bencsura and G. Lendvay, Bimolecular Reactions of Vibrationally Excited Molecules. Roaming Atom Mechanism at Low Kinetic Energies, *J. Phys. Chem. A*, 2012, **116**(18), 4445–4456, DOI: 10.1021/jp301243a.

43 T. Endo, S. P. Neville, V. Wanie, S. Beaulieu, C. Qu, J. Deschamps, P. Lassonde, B. E. Schmidt, H. Fujise, M. Fushitani, A. Hishikawa, P. L. Houston, J. M. Bowman, M. S. Schuurman, F. Légaré and H. Ibrahim, Capturing Roaming Molecular Fragments in Real Time, *Science*, 2020, **370**(6520), 1072–1077, DOI: 10.1126/science.abc2960.

44 T. Severt, D. R. Daugaard, T. Townsend, F. Ziaee, K. Borne, S. Bhattacharyya, K. D. Carnes, D. Rolles, A. Rudenko, E. Wells and I. Ben-Itzhak, Two-Body Dissociation of Formic Acid Following Double Ionization by Ultrafast Laser Pulses, *Phys. Rev. A*, 2022, **105**(5), 053112, DOI: 10.1103/PhysRevA.105.053112.

45 S. Maeda, T. Taketsugu and K. Morokuma, Automated Exploration of Photolytic Channels of HCOOH: Conformational Memory *via* Excited-State Roaming, *J. Phys. Chem. Lett.*, 2012, **3**(14), 1900–1907, DOI: 10.1021/jz300728q.

46 Y. Ma, J. Liu, F. Li, F. Wang and T. N. Kitsopoulos, Roaming Dynamics in the Photodissociation of Formic Acid at 230 Nm, *J. Phys. Chem. A*, 2019, **123**(17), 3672–3677, DOI: 10.1021/acs.jpca.9b00724.

47 K. C. Lin, C. J. Tso and T. Kasai, Beyond the Rule of Transition State: Identification of Roaming Routes in Some Cases of Carbonyl Compounds, *J. Chin. Chem. Soc.*, 2021, **68**(8), 1358–1378, DOI: 10.1002/jccs.202100039.

48 C. J. Tso, T. Kasai and K. C. Lin, Roaming Dynamics and Conformational Memory in Photolysis of Formic Acid at 193 Nm Using Time-Resolved Fourier-Transform Infrared Emission Spectroscopy, *Sci. Rep.*, 2020, **10**(1), 4769, DOI: 10.1038/s41598-020-61642-7.

49 T. Liu, S. N. Elliott, M. Zou, M. F. Vansco, C. A. Sojdak, C. R. Markus, R. Almeida, K. Au, L. Sheps, D. L. Osborn, F. A. F. Winiberg, C. J. Percival, C. A. Taatjes, R. L. Caravan, S. J. Klippenstein and M. I. Lester, OH Roaming and Beyond in the Unimolecular Decay of the Methyl-Ethyl-Substituted Criegee Intermediate: Observations and Predictions, *J. Am. Chem. Soc.*, 2023, **145**(35), 19405–19420, DOI: 10.1021/jacs.3c07126.

50 S. J. Klippenstein and S. N. Elliott, OH Roaming during the Ozonolysis of α-Pinene: A New Route to Highly Oxygenated Molecules, *J. Phys. Chem. A*, 2023, **127**(50), 10647–10662, DOI: 10.1021/acs.jpca.3c05179.

51 P. Del Mazo-Sevillano, A. Aguado, E. Jiménez, Y. V. Suleimanov and O. Roncero, Quantum Roaming in the Complex-Forming Mechanism of the Reactions of OH with Formaldehyde and Methanol at Low Temperature and Zero Pressure: A Ring Polymer Molecular Dynamics Approach, *J. Phys. Chem. Lett.*, 2019, **10**(8), 1900–1907, DOI: 10.1021/acs.jpclett.9b00555.

52 Z. Li, Y. Fu, Z. Luo, S. Yang, Y. Wu, H. Wu, G. Wu, W. Zhang, B. Fu, K. Yuan, D. Zhang and X. Yang, Roaming in Highly Excited States: The Central Atom Elimination of Triatomic Molecule Decomposition, *Science*, 2024, **383**(6684), 746–750, DOI: 10.1126/science.adn3357.

53 E. Kamarchik, L. Koziol, H. Reisler, J. M. Bowman and A. I. Krylov, Roaming Pathway Leading to Unexpected Water + Vinyl Products in C 2H4OH Dissociation, *J. Phys. Chem. Lett.*, 2010, **1**(20), 3058–3065, DOI: 10.1021/jz1011884.

54 B. R. Heazlewood, M. J. T. Jordan, S. H. Kable, T. M. Selby, D. L. Osborn, B. C. Shepler, B. J. Braams and J. M. Bowman, Roaming Is the Dominant Mechanism for Molecular Products in Acetaldehyde Photodissociation, *Proc. Natl. Acad. Sci. U. S. A.*, 2008, **105**(35), 12719–12724, DOI: 10.1073/pnas.0802769105.

55 N. B. Bejoy, P. Roy Chowdhury and G. N. Patwari, Modulating the Roaming Dynamics for the NO Release in Ortho-Nitrobenzenes, *J. Phys. Chem. Lett.*, 2023, **14**(11), 2816–2822, DOI: 10.1021/acs.jpclett.3c00134.

56 T. Matsubara, Dynamic Effects on the Ionization-Induced Reactions of Methyl Halides: Quantum Mechanical and Molecular Dynamics Studies, *J. Phys. Chem. A*, 2023, **127**(22), 4801–4814, DOI: 10.1021/acs.jpca.3c01669.

57 J. Zhou, S. Jia, X. Hu, E. Wang, X. Xue, Y. Wu, J. Wang, A. Dorn and X. Ren, Intermolecular Charge Transfer Induced Fragmentation of Formic Acid Dimers, *Phys. Rev. Lett.*, 2023, **130**(23), 233001, DOI: 10.1103/PhysRevLett.130.233001.

58 J. Zhou, S. Jia, A. D. Skitnevskaya, E. Wang, T. Hähnel, E. K. Grigoricheva, X. Xue, J. X. Li, A. I. Kuleff, A. Dorn and X. Ren, Concerted Double Hydrogen-Bond Breaking by Intermolecular Coulombic Decay in the Formic Acid Dimer, *J. Phys. Chem. Lett.*, 2022, **13**(19), 4272–4279, DOI: 10.1021/acs.jpclett.2c00957.

59 K. Hoshina, H. Hagihara and M. Tsuge, Double Ionization and Coulomb Explosion of the Formic Acid Dimer by Intense Near-Infrared Femtosecond Laser Pulses, *J. Phys. Chem. A*, 2012, **116**(2), 826–831, DOI: 10.1021/jp2111154.

60 I. Luzon, E. Livshits, K. Gope, R. Baer and D. Strasser, Making Sense of Coulomb Explosion Imaging, *J. Phys. Chem. Lett.*, 2019, **10**(6), 1361–1367, DOI: 10.1021/acs.jpclett.9b00576.

61 I. Luzon, K. Jagtap, E. Livshits, O. Lioubashevski, R. Baer and D. Strasser, Single-Photon Coulomb Explosion of Methanol Using Broad Bandwidth Ultrafast EUV Pulses, *Phys. Chem. Chem. Phys.*, 2017, **19**(21), 13488–13495, DOI: 10.1039/c7cp00587c.

62 D. M. Bittner, K. Gope, E. Livshits, R. Baer and D. Strasser, Sequential and Concerted C-C and C-O Bond Dissociation in the Coulomb Explosion of 2-Propanol, *J. Chem. Phys.*, 2022, **157**(7), 074309, DOI: 10.1063/5.0098531.

63 D. M. Bittner, K. Gope and D. Strasser, Time-Resolved Dissociative Ionization and Double Photoionization of CO2, *J. Chem. Phys.*, 2020, **153**(19), 194201, DOI: 10.1063/5.0028812.
64 N. Ekanayake, M. Nairat, B. Kaderiya, P. Feizollah, B. Jochim, T. Severt, B. Berry, K. R. Pandiri, K. D. Carnes, S. Pathak, D. Rolles, A. Rudenko, I. Ben-Itzhak, C. A. Mancuso, B. S. Fales, J. E. Jackson, B. G. Levine and M. Dantus, Mechanisms and Time-Resolved Dynamics for Trihydrogen Cation (H3+) Formation from Organic Molecules in Strong Laser Fields, *Sci. Rep.*, 2017, **7**(1), 4703, DOI: 10.1038/s41598-017-04666-w.
65 H. Xu, T. Okino, T. Kudou, K. Yamanouchi, S. Roither, M. Kitzler, A. Baltuska and S. L. Chin, Effect of Laser Parameters on Ultrafast Hydrogen Migration in Methanol Studied by Coincidence Momentum Imaging, *In J. Phys. Chem. A*, 2012, **Vol. 116**, 2686–2690, DOI: 10.1021/jp207483y.
66 T. Ando, A. Shimamoto, S. Miura, A. Iwasaki, K. Nakai and K. Yamanouchi, Coherent Vibrations in Methanol Cation Probed by Periodic H3+ Ejection after Double Ionization, *Commun. Chem.*, 2018, **1**, 7, DOI: 10.1038/s42004-017-0006-7.
67 L. S. Cederbaum, J. Zobeley and F. Tarantelli, Giant Intermolecular Decay and Fragmentation of Clusters, *Phys. Rev. Lett.*, 1997, **79**(24), 4778–4781, DOI: 10.1103/PhysRevLett.79.4778.
68 C. Wang, B. Wang, M. Okunishi, W. G. Roeterdink, D. Ding, R. Zhu, G. Prümper, K. Shimada and K. Ueda, Ion-Ion Coincidence Imaging of Dissociative Ionization Dynamics of Formic Acid in Intense Laser Fields, *Chem. Phys.*, 2014, **430**, 40–46, DOI: 10.1016/j.chemphys.2013.12.003.
69 T. R. Huet, C. J. Pursell, W. C. Ho, B. M. Dinelli and T. Oka, Infrared Spectroscopy and Equilibrium Structure of H2O +(X̃2B1), *J. Chem. Phys*, 1992, **97**(9), 5977–5987, DOI: 10.1063/1.463735.
70 D. Liu, C. Zhang, X. Hao, X. Xue, M. Gong, S. Zhang, J. Zhou, C. Kong, Z. Yang, X. Ren and T. Yang, On-the-Fly Nonadiabatic Molecular Dynamics Reveals Dissociation Mechanisms of Multiply Charged Molecules, *Phys. Rev. Lett.*, 2026, **136**(12), 123202, DOI: 10.1103/c8yq-fzn5.
71 A. Bogot, M. Poline, M. C. Ji, A. Dochain, S. Rosén, H. Zettergren, H. T. Schmidt, R. D. Thomas and D. Strasser, Unravelling Non-Adiabatic Pathways in the Mutual Neutralization of Hydronium and Hydroxide, *Nat. Chem.*, 2025, **17**(4), 541–546, DOI: 10.1038/s41557-025-01771-6.
72 J. R. Sutherland, E. L. Christensen, N. D. Powers, S. E. Rhynard, J. C. Painter and J. Peatross, High Harmonic Generation in a Semi-Infinite Gas Cell, *Opt. Express*, 2004, **12**(19), 4430, DOI: 10.1364/OPEX.12.004430.
73 J. P. Brichta, M. C. H. Wong, J. B. Bertrand, H. C. Bandulet, D. M. Rayner and V. R. Bhardwaj, Comparison and Real-Time Monitoring of High-Order Harmonic Generation in Different Sources, *Phys. Rev. A*, 2009, **79**(3), 033404, DOI: 10.1103/PhysRevA.79.033404.
74 D. M. Kandhasamy, Y. Albeck, K. Jagtap and D. Strasser, 3D Coincidence Imaging Disentangles Intense Field Double Detachment of SF6, *J. Phys. Chem. A*, 2015, **119**(29), 8076–8082, DOI: 10.1021/acs.jpca.5b04101.
75 X. Urbain, D. Bech, J. P. Van Roy, M. Géléoc, S. J. Weber, A. Huetz and Y. J. Picard, A Zero Dead-Time Multi-Particle Time and Position Sensitive Detector Based on Correlation between Brightness and Amplitude, *Rev. Sci. Instrum.*, 2015, **86**(2), 023305, DOI: 10.1063/1.4908597.
76 S. K. Lee, F. Cudry, Y. F. Lin, S. Lingenfelter, A. H. Winney, L. Fan and W. Li, Coincidence Ion Imaging with a Fast Frame Camera, *Rev. Sci. Instrum.*, 2014, **85**(12), 123303, DOI: 10.1063/1.4903856.
77 A. Shahi, Y. Albeck and D. Strasser, Simultaneous 3D Coincidence Imaging of Cationic, Anionic, and Neutral Photo-Fragments, *Rev. Sci. Instrum.*, 2018, **89**(1), 013303, DOI: 10.1063/1.5004523.
78 E. Livshits and R. Baer, A Well-Tempered Density Functional Theory of Electrons in Molecules, *Phys. Chem. Chem. Phys.*, 2007, **9**(23), 2932–2941, DOI: 10.1039/b617919c.
79 R. Baer, E. Livshits and U. Salzner, Tuned Range-Separated Hybrids in Density Functional Theory, *Annu. Rev. Phys. Chem.*, 2010, **61**, 85–109, DOI: 10.1146/annurev.physchem.012809.103321.
80 E. Livshits, R. S. Granot and R. Baer, A Density Functional Theory for Studying Ionization Processes in Water Clusters, *J. Phys. Chem. A*, 2011, **115**(23), 5735–5744, DOI: 10.1021/jp1057572.
81 Y. Shao, *et al.*, Advances in Molecular Quantum Chemistry Contained in the Q-Chem 4 Program Package, *Mol. Phys.*, 2015, **113**(2), 184–215, DOI: 10.1080/00268976.2014.952696.
82 J. C. Tully, Molecular Dynamics with Electronic Transitions, *J. Chem. Phys*, 1990, **93**(2), 1061–1071, DOI: 10.1063/1.459170.
83 T. Shiozaki, BAGEL: Brilliantly Advanced General Electronic-Structure Library, *Wiley Interdiscip. Rev. Comput. Mol. Sci.*, 2018, **8**(1), 1061–1071, DOI: 10.1002/wcms.1331.
84 J. Finley, A. Malmqvist, B. O. Roos, L. Serrano-Andrés and A. Andrés, The Multi-State CASPT2 Method, *Chem. Phys. Lett.*, 1998, **288**, 299–306, DOI: 10.1016/S0009-2614(98)00252-8.
85 B. Vlaisavljevich and T. Shiozaki, Nuclear Energy Gradients for Internally Contracted Complete Active Space Second-Order Perturbation Theory: Multistate Extensions, *J. Chem. Theory Comput.*, 2016, **12**(8), 3781–3787, DOI: 10.1021/acs.jctc.6b00572.
86 M. Barbatti, M. Ruckenbauer, F. Plasser, J. Pittner, G. Granucci, M. Persico and H. Lischka, Newton-X: A Surface-Hopping Program for Nonadiabatic Molecular Dynamics, *Wiley Interdiscip. Rev. Comput. Mol. Sci.*, 2014, **4**(1), 26–33, DOI: 10.1002/wcms.1158.
87 J. W. Park and T. Shiozaki, On-the-Fly CASPT2 Surface-Hopping Dynamics, *J. Chem. Theory Comput.*, 2017, **13**(8), 3676–3683, DOI: 10.1021/acs.jctc.7b00559.